COMMUNICATION

Reduced Energetic Disorders in Dion-Jacobson Perovskites for Efficient and Spectral Stable Blue LEDs

Jisung Seo[a,f], Kang Wang*[a,f], Aidan H. Coffey[b], Guiying He[c,d], Hanjun Yang[a], Yoon Ho Lee[a], Ke Ma[a], Jiaonan Sun[a], Jee Yung Park[a], Han Zhao[a], Chongli Yuan[a], Chenhui Zhu[b], Matthew Y. Sfeir[c,d], and Letian Dou*[a,e]

[a]   J. Seo, Dr. K. Wang, Dr. H. Yang, Dr. Y. H. Lee, Dr. K. Ma, Dr. J. Sun, J. Y. Park, H. Zhao, Prof. C. Yuan, Prof. L. Dou
        Davidson School of Chemical Engineering
        Purdue University
        West Lafayette, IN 47907, USA
        *E-mail: dou10@purdue.edu; wang4604@purdue.edu
[b]   Dr. A. Coffey, Dr. C. Zhu
        Advanced Light Source
        Lawrence Berkeley National Laboratory
        Berkeley, CA 94720, USA
[c]   Dr. G. He, Prof. M. Sfeir
        Department of Physics, Graduate Center
        City University of New York
        New York, NY, 10016 USA
[d]   Dr. G. He, Prof. M. Sfeir
        Photonics Initiative, Advanced Science Research Center
        City University of New York
        New York, NY 10031 USA
[e]   Prof. L. Dou
        Birck Nanotechnology Center
        Purdue University
        West Lafayette, IN 47907, USA
[f]   These authors contributed equally.

        Supporting information for this article is given via a link at the end of the document.

Abstract: Metal halide perovskites have witnessed great success in green, red, and near-infrared light-emitting diodes (LEDs), yet blue LEDs still lag behind. Reducing undesired energetic disorders - broad n-phases and halide segregation – is considered as the most critical strategy to further improve the performances. Here, we report a newly designed and synthesized di-ammonium ligand with rigid π-conjugated rings and additional methyl groups to construct Dion-Jacobson (DJ) structure. Augmented coordination from the extra ammonium site and increased effective bulkiness from methyl groups lead to better distribution control over conventional mono-ammonium ligands. This enhances the radiative recombination of blue emissions in the film with homogeneous energy landscape and improved surface morphology, as evidenced by a series of imaging and mapping techniques. As a result, we demonstrated DJ perovskite LEDs (PeLEDs) with peak external quantum efficiencies of ~4% at 484 nm and ~11% at 494 nm, which are among the top reported for pure DJ phase based PeLEDs in the corresponding wavelength regions. Our results deepen the understanding of regulating energetic disorders in perovskite materials via molecular engineering.

Metal halide perovskites are emerging as promising candidates for next-generation light-emitting diodes (LEDs) due to their compelling color purity, excellent tunability, and outstanding optoelectronic properties.[1] The external quantum efficiencies (EQEs) of green, red, and near-infrared perovskite LEDs

(PeLEDs) have surpassed 20% along with their advancement in operational stabilities.[2] Blue PeLEDs, however, considerably fall behind in performances due to their intrinsic wide bandgap and unfavorable nonradiative recombination.[3] Two-dimensional (2D) or quasi-2D perovskite structure is recognized as a versatile platform that most PeLEDs have adapted to enhance their device performances,[4] in which the incorporated large organic ligands create quantum confinement for charge carriers to recombine radiatively, thus representing an encouraging strategy to boost the blue PeLEDs performances. The pitfall of quasi-2D perovskites is the broad n-phases that may cause inefficient energy transfer from wide bandgap to low bandgap components, ultimately resulting in low-energy emissions away from the blue region.[5] Accordingly, n-phase control is an essential aspect of ensuring efficient and color-pure blue PeLEDs.[6] In addition, a Br^- and Cl^- mixed halide system for blue PeLEDs generally suffers from considerable halide segregations under external stimuli, such as light, heat, or bias voltage, which may lead to nonhomogeneous halide distribution and unstable device operation.[7] Therefore, pernicious drawbacks impeding the high-performance and spectral stable blue PeLEDs must be overcome by mitigating those energetic disorders in terms of broad n-phases and halide segregation.

It is well-accepted that bulky or coordinating organic ligands could slow down or even prevent the facile diffusion of ionic species

during the crystallization process.[2a, 8] This could assist composition-control of quasi-2D perovskites by inhibiting the formation of divergent low *n*-phase and 3D phase.[2a, 9] Nonetheless, simply increasing the ligand size for blue PeLEDs is inadequate as the ligands with extended π-conjugated systems exhibit narrow band gaps that are prone to absorbing high-energy emissions. Dion-Jacobson (DJ) perovskite structure formed with di-ammonium ligands may enable a better control over *n*-phases without causing extra energy loss.[10] Di-ammonium ligands – compared to the conventional mono-ammonium ligands in Ruddlesden-Popper (RP) phase perovskites – possess an additional ammonium group, which would result in augmented coordination with surrounding precursors.[11] Moreover, the DJ phase configuration enhances the structural rigidity among superlattices with hydrogen bonding and eliminates the ligand-ligand interface that exists in the RP phase[12], which may reinforce tolerance from external stimuli and constructively suppress spatial disorders.

In this work, to investigate intriguing properties of di-ammonium ligands toward reduced energetic disorders and the advantages of the DJ phase perovskite structure for blue PeLEDs, we designed and synthesized two novel di-ammonium conjugated ligands. In comparison with the mono-ammonium case, the as-fabricated perovskite thin films with di-ammonium ligands show blue shifted emissions, higher photoluminescence quantum yield (PLQY), and reduced surface roughness, which are beneficial for LED applications. Combined structural and compositional analysis helped us confirm that better *n*-phase control and suppressed halide segregation provided by di-ammonium ligands were highly responsible for those improved film properties. On this basis, our PPm-based PeLEDs exhibit peak EQEs of 3.8% at 484 nm and 10.6% at 494 nm, which are among the top reported for pure DJ phase based PeLEDs in the corresponding wavelength regions.[10a, 13] Our findings indicate that incorporating di-ammonium ligands is an effective strategy to reduce energetic disorders in perovskite materials for efficient blue PeLEDs.

Figure 1a illustrates the general structures of RP and DJ phase perovskites. It should be noted that the ligand-ligand interface in RP phase will no longer exist in DJ phase. Phenylethylammonium bromide (PEA), a typical mono-ammonium ligand used in RP phase, was selected as a reference in this work. Two new di-ammonium ligands, [1,1'-biphenyl]-4,4'-dimethylammonium bromide (PP) and 2,2'-dimethyl-[1,1'-biphenyl]-4,4'-dimethylammonium bromide (PPm), were synthesized by following the procedures detailed in Supporting Information. Briefly, PP and PPm were obtained via reduction reaction with an organosilane reductant in the presence of tris(pentafluorophenyl)borane Lewis acid, and protonation with hydrobromide acid, from biphenyl based di-carbonitrile precursors. The biphenyl di-carbonitrile precursors with and without methyl group can both be synthesized from boronic acid and aryl bromide by Suzuki-Miyaura cross-coupling reactions in high yield.[14] The target ligands were characterized by ^{1}H and ^{13}C nuclear magnetic resonance (NMR) spectroscopy and mass spectrometry (MS). One should note that rigid π-conjugated phenyl rings were inserted to promote charge carrier injection while inhibit ion migration with increased bulkiness.[15] The use of mono-carbon linkers between the biphenyl backbone and ammonium tails aims to decrease electrical resistance, and at the same time, maintain

the molecular symmetry.[13b] Notably, the methyl groups attached at 2- and 2'-positions in PPm further increase the steric hindrance of the ligand to maximize bulkiness. This is expected to slow down the crystallization process of perovskite films, leading to more homogeneous *n*-phases and halides distribution.[8]
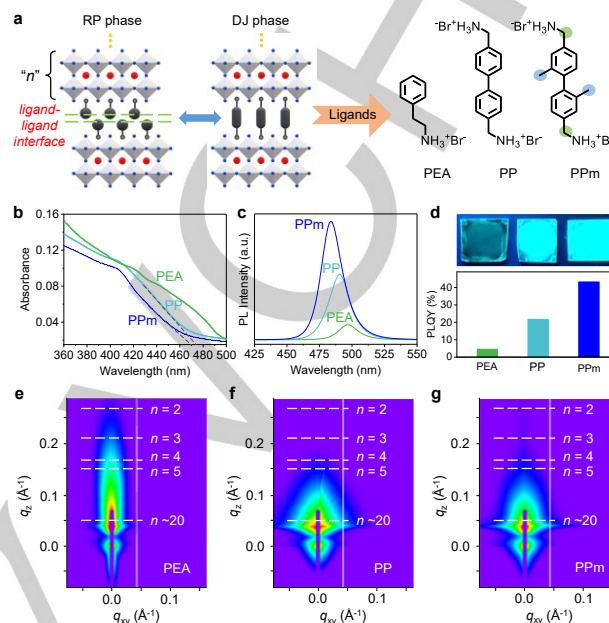

Figure 1. a) The schematic illustration of the quasi-2D RP and DJ phase perovskite structures and the chemical structure of conjugated ligands, PEA, PP, and PPm. The "*n*" is the number of inorganic layers sandwiched between organic ligands. **b)** Absorption and **c)** PL spectra of PEA, PP, and PPm based quasi-2D perovskite thin films. A Br⁻ and Cl⁻ mixed halide system is employed in this work. **d)** Photographs and PLQY of perovskite thin films fabricated from PEA (left), PP (middle), and PPm (right). GISAXS measurement of **e)** PEA, **f)** PP, and **g)** PPm-based films. q_z and q_{xy} represent the out-of-plane and in-plane scattering vectors, respectively. The white dash lines indicate different *n*-phase diffractions along q_z direction. Note, there are some obscure diffractions at q_z~0.2 A⁻¹ in (g), which are absent in (f), suggesting that a tiny amount of *n* = 3 may coexist in PPm film.

As shown in **Figure 1b**, the absorption of PEA based thin film sample shows an onset at ~490 nm, while both PP and PPm show blue shifted onset at ~470 nm. The PL spectra of PP- and PPm-based thin films are centered at 491 and 483 nm, respectively, which are also blue-shifted compared with the PEA sample (497 nm, **Figure 1c**). The absorption and PL data altogether suggest that the application of di-ammonium ligands, PP and PPm, suppressed the segregation that forms higher *n* components (more analysis on ligand effects can be found in Figure S1). Moreover, PP and PPm-based films achieved higher PL intensities with an enhanced PLQY of 21.7 and 43.2%, respectively, in comparison with the PEA case (PLQY~4.5%, **Figure 1c, d**). These further support that the di-ammonium ligands may have successfully alleviated the divergent phase distribution and lowered defect densities that could cause inefficient energy transfer and substantial non-radiative recombination.[2a, 16] In contrast with the PP case, PPm sample showed more blue-shifted absorption and PL peak as well as improved PLQY. This could be attributed to the two added methyl groups that increase the effective bulkiness of PPm ligand and augmented coordination with precursors. In crystallization kinetics,

the less bulky and coordinating ligands tend to diffuse more readily than bulkier and highly coordinating ones, thus reducing n-phase segregation and form quantum wells with controlled slab thickness (n number).[17]

Thin film X-ray diffraction (XRD) and grazing-incidence small-angle X-ray scattering (GISAXS) were carried out to examine the structural information of perovskite films. We conducted XRD for the 2D perovskite thin films made from n = 1 precursor solutions with different ligands, where the molar ratios of PEA, PP, PPm to $PbBr_2$ are 2:1, 1:1, 1:1, respectively. Both PP and PPm exhibit a set of characteristic peaks that are identical to those of PEA (Figure S2). This indicates that all the perovskite films resulting from PEA, PP, and PPm ligands share the same d-spacings, confirming the formation of DJ phase structure from PP and PPm ligands. The GISAXS measurements were then performed on the blue emissive perovskite films with their composition included in Supporting Information. As shown in **Figure 1e**, the PEA-based perovskite showed broad n ranging from n = 2 to a much higher n based on the patterns along out-of-plane (q_z) direction. Surprisingly, for PP and PPm ligands, there are no obvious diffractions corresponding to n = 1-3 in **Figure 1f** and **g**, validating the suppression of low-n phases.[8, 18] Furthermore, the scattering pattern of PP film discloses a broad profile along in-plane (q_{xy}) direction whereas PPm-based film shows a relatively narrow one (**Figure 2b, c**). This sharp distribution profile of PPm film suggests better crystallinity and improved energy landscape homogeneity.
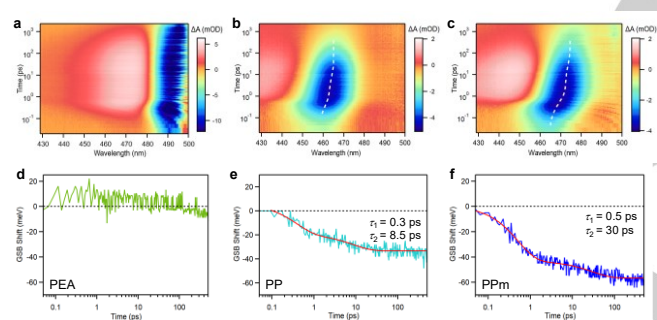

Figure 2. a-c) Pseudo color maps of TA spectra for (a) PEA, (b) PP, and (c) PPm based films. The dotted lines on the 2D raw data plots indicate the GSB minimum at different delay time. **d-f**) The magnitude of the GSB shifts in meV as a function of time along with a bi-exponential fit for PP and PPm.

Transient absorption (TA) spectroscopy measurements[19] were carried out on quasi-2D perovskite films to probe the homogeneity in energy landscape and the corresponding charge carrier dynamics (**Figure 2**). PEA shows that the low energy sites (high-n phase) are populated rapidly (**Figure 2a**) as indicated by a ground state bleach (GSB) signal near 490 nm. The GSB spectral position is relatively constant as a function of time, indicating that there is no transport of excitons among sites with different phases. Together with the PL low quantum yield and spatially-resolved PL measurements (**Figure 3a,d**), these data suggest that carriers created outside of a few dominant spatial locations are extremely promptly quenched. This prevents energy relaxation over long distances despite the large distribution of nonhomogeneous energy sites in PEA film (**Figure 1e**). In contrast, both PP and PPm exhibit a continual red shift of the GSB minimum with time that persists over long timescales (up to 10s of ps) (**Figure 2b,c**).

The magnitude of the red shift in PPm is larger (~ 60 meV) and the time scale for relaxation is slower (time constants of ~ 0.5 ps and 30 ps) compared to PP (~ 30 meV, 0.33 ps and 8.5 ps) (**Figure 2e,f**). The higher PLQY in PP and PPm (**Figure 1d**) suggests that this observation of slow carrier cooling in PPm is consistent with their lower defect densities and more homogeneous energy landscapes that facilitates the transport of charge carriers. The TA spectrum of PP is blue shifted compared with that of PPm, which has the opposite trend as shown in the steady state absorption spectra (**Figure 1b**). Here, the energetic disorders would have limited the transport of charge carriers within the wide-bandgap grains that were initially populated, thus leading to TA signals from lower-n phases and blue-shifted spectral feature in PP film. Furthermore, the position of the GSB in PP and PPm at long delay times, corresponding to "cooled" states, are blue shifted compared with PEA, again implying the suppression of high-n phases.

To comprehensively interpret the spatial energetic disorders in the quasi-2D perovskite films, we employed a series of imaging and mapping techniques. First, fluorescence-lifetime imaging microscopy (FLIM) was conducted to investigate the disorders of excitonic properties in perovskite films. As shown in **Figure 3a, b**, the island-like features formed in PEA and PP suggest nonhomogeneous distribution that potentially deactivates the energy transfer pathway, resulting in a relatively low PL intensity. While in PPm film, its superior PL intensity and consistent fluorescence mapping (**Figure 3c**) reveal well-controlled n-phases and more efficient radiative recombination. More importantly, the FLIM results exhibit an extended lifetime of excitons for PP and PPm films (**Figure 3e, f**). As defects throughout the grains can rapidly dissipate the excitons, the longer lifetimes imply the reduced defect density compared to the PEA film (**Figure 3d**). These align well with the TA results.
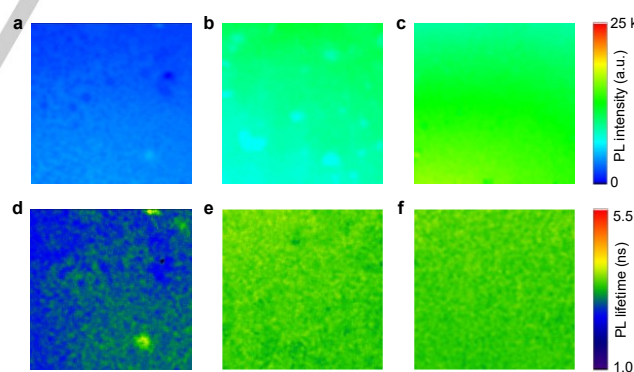
Figure 3. FLIM images for **a-c**) PL intensity and **d-f**) the corresponding PL lifetime of (a,d) PEA, (b,e) PP, and (c,f) PPm films. The area of all the images is 30 × 30 μm.

Next, Kelvin probe force microscope (KPFM) measurements were utilized to visualize the disorders in morphology and surface potential. As displayed in the atomic force microscope (AFM) height profile, the PEA thin film manifests inhomogeneous and discrete grains with a root-mean-square (r.m.s) roughness of ~2.98 nm (**Figure 4a**), revealing undesired crystallization process. In contrast, continuous grains with smaller size and reduced roughness are observed from PP and PPm thin films (r.m.s.,

~0.95 and 0.86 nm, respectively, **Figure 4b, c,**). The improved surface morphology is correlated with the slower crystallization due to augmented coordination provided by di-ammonium ligands.[13a, 20] The more uniform surface and smaller grain size of PP and PPm film could have alleviated energetic disorder and induced quantum confinement for perovskites, resulting in enhanced photoluminescence along with stable blue emissions. As shown in **Figure 4d, e**, the contact potential difference (CPD) map of PEA and PP-based thin films exhibit substantial heterogeneity in surface potentials, which matches up with the spatial energetic disorders (see more discussion in Method part). While the CPD map of PPm film exhibits the most pronounced uniformity (**Figure 4f**), indicating more homogenous distribution of *n*-phases and halides.

Energy-dispersive X-ray spectroscopy (EDX) through scanning electron microscope (SEM) was further employed to illustrate the disorders in halide distribution and understand how halide distribution can be mitigated by the selection of organic ligands. The dominant source of unpredictable and unstable device operation for blue LEDs is generally considered to be halide segregation, which is driven by traps, unfavorable stoichiometric ratio of mixed halides, or nonhomogeneous distribution of *n*-phases.[7b] While the SEM images did not reveal obvious morphology disorders among different films (Figure S3), substantial heterogeneity was observed from Br and Cl distribution in EDX for PEA sample (**Figure 4g**). The relatively more uniform Br and Cl distributions from the PP and PPm samples (**Figure 4h and i**), again confirm the reduced energetic disorders by di-ammonium ligands in DJ perovskites.
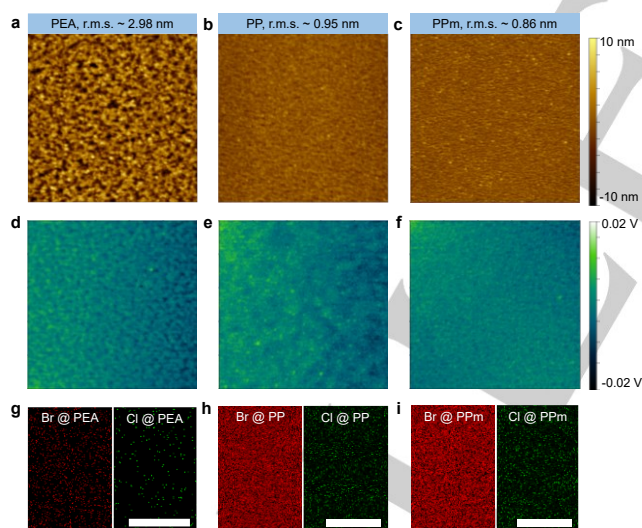

Figure 4. a-c) AFM topography, **d-f)** KPFM CPD images, and **g-i)** elemental mapping of bromine (Br^L) and chlorine (Cl^K) for perovskite films fabricated from different ligands, (a,d,g) PEA, (b,e,h) PP, and (c,f,i) PPm. The areas of (a-d) are 5 μm × 5 μm. The scale bars in (g-i) are 500 nm.

We further tracked steady-state PL of the PEA, PP, and PPm-based perovskite films with photo-irradiation and thermal annealing. Under constant light irradiation, the PEA-based film appreciably red-shifted after 30 minutes (Figure S4a), indicating that halide segregation had occurred.[21] The PP and PPm-based films show only slight shifts under irradiation (Figure S4b,c). As

for the thermal annealing study, continuous shift was observed for PEA film from 50 to 110 °C (Figure S4d), and minor shift from 50 to 90 °C and drastic red shift at 110 °C can be noticed from PP film (Figure S4e). The shifts at different temperatures are insignificant for PPm-based film (Figure S4f), further supporting that PPm is better than PP and PEA in terms of suppressing both *n*-phase and halide segregation.[16]

Ex-situ absorption and PL spectra were measured by annealing perovskite films at 110 °C for different times to understand the function of large ligands in controlling the crystallization pathways of quasi-2D perovskites. Before thermal annealing, all three ligands show the absorption and emissions at blue regions (black dash curves in Figure S5), indicating homogeneous halide distribution and median *n*-phases in the film. During thermal annealing, secondary growth of the grain will occur via thermal energy driven ion diffusion, resulting in the emergence of high *n*-phases in the film. Particularly, drastic red shifts with time were observed for both PEA and PP samples (solid curves in Figure S5a,b,d,e). While the shift for PPm was less significant (solid curves in Figure S5c,f), suggesting suppressed secondary growth. Therefore, we can summarize a crystallization model for quasi-2D perovskites, where ligands play an important role in regulating interlayer ion migration and ultimately the kinetics of *n*-phases and halide segregations (Figure S6). The pivotal factor that PPm has over the PP cation is the methyl groups at 2,2'-positions that can give rise to enhanced steric hinderance. This could better suppress the ion migration through spacings of ligand layer as highlighted by the red arrows in Figure S6b,c and S7[16], thus leading to reduced energetic disorders. Although ions can migrate through other pathways and eventually affect the crystallization kinetics, the ion diffusion through interlayer spacings proposed in this work provides a good rationale for the suppression of *n*-phase and halide segregation in this typical blue system.
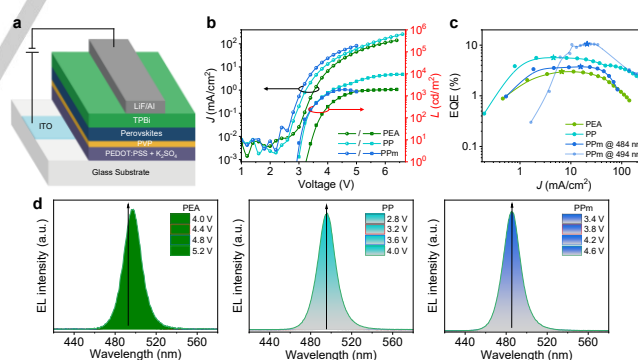
Figure 5. a) PeLED device structure. **b)** Current density versus voltage (*J-V*) and luminance versus voltage (*L-V*) curves. **c)** EQE versus current density characteristic curves and **d)** electroluminescence (EL) spectra at different driving voltages for PEA, PP, and PPm devices.

To evaluate the device performance of di-ammonium quasi-2D perovskite, we fabricated PeLEDs with the device structure shown in **Figure 5a**. The device configuration is arranged as indium tin oxide (ITO, anode)/PEDOT:PSS (with K_2SO_4, hole transport layer, ~40 nm)/polyvinylpyrrolidone (PVP, interlayer, sub-nanometer)/quasi-2D perovskites (active layer, ~30 nm)/1,3,5-tris(1-phenyl-1H-benzimidazol-2-yl)benzene (TPBi, electron transport layer, ~40 nm)/lithium fluoride (LiF, electron

injection layer, ~1.2 nm)/aluminum (Al, cathode, ~100 nm). Ultrathin PVP was introduced as an interlayer to mitigate the potential interfacial loss between acidic PEDOT:PSS and perovskites. As shown in Figure S8 and S9 in the Supporting Information, by introducing PVP layer, the emission intensity and wavelength are enhanced and blue-shifted respectively, which is favorable for blue LEDs. The turn-on voltage for *J-V* and luminance curves for all PP-, and PPm-based PeLEDs match well around 2.8 V, indicating that the charge injection for electrons and holes is mostly balanced (**Figure 5b**). The peak EQEs of PP- and PPm-based PeLEDs achieved in this work are 5.7% and 3.8% (**Figure 5c**), along with their EL emission centered at 494 nm and 484 nm, respectively. PEA device achieved comparatively low 3.0% EQE at 500 nm, which is likely attributed to the uncontrolled phase distribution and unregulated energetic disorders. Surface passivation agents or molecular modifiers have been widely reported to better control the phase distribution and energetic disorders towards highly efficient PEA-based blue LEDs.[4d, 6, 22] More importantly, PPm devices delivered a peak EQE of 10.6% at 494 nm (light blue curve in **Figure 5c** and Figure S10), suggesting that our di-ammonium ligand is also similarly efficient in controlling energetic disorders for efficient blue PeLEDs.

In addition, the spectral stability test of PEA device has shown substantial EL shifting from 490 nm to 500 nm upon increasing the driving voltages (**Figure 5d**). This spectral shift is normally observed from conventional RP phase PeLEDs caused by ion migration under bias voltage.[5b] In contrast, for PP- and PPm-based devices, no obvious spectral shifting is observed, which again confirms superior device performance and stability by adopting effective di-ammonium ligands. Additionally, the PPm device shows more than three times enhanced operational stability compared to PEA and PP devices (Figure S11). This stability is much better than that of the other di-ammonium based DJ phase blue PeLEDs[10a, 13a-c] and even on par with the most recently reported highly efficient mono-ammonium based RP phase PeLEDs in blue regions.[22-23]

In summary, we have demonstrated that di-ammonium ligands could naturally provide a better distribution control compared to conventional mono-ammonium ligand by augmented coordination with other ionic species during solution processing, which ultimately alleviates the energy landscape heterogeneity and reduces defect densities. Two extra methyl groups introduced to the novel di-ammonium ligand could induce a steric hindrance for DJ phase perovskites. This allows a more homogeneous distribution evident from a series of structural and compositional analysis methods, thus resulting in blue-shifted emission, improved surface morphology, and enhanced optoelectronic properties. Consequently, we achieved a peak EQE of 3.8% at 484 nm and 10.6% for at 494 nm based on DJ phase perovskites. Furthermore, the spectral stable emissions further confirm the outstanding properties of this novel di-ammonium ligand and the DJ perovskite structure. We anticipate our investigation into the properties of di-ammonium ligands and strategies toward functional ligand design will extend the understanding toward achieving highly efficient and stable blue as well as other color PeLEDs.

Acknowledgements

Conflict of interest

The authors declare no conflict of interest.

[1] a) Z.-K. Tan, R. S. Moghaddam, M. L. Lai, P. Docampo, R. Higler, F. Deschler, M. Price, A. Sadhanala, L. M. Pazos, D. Credgington, F. Hanusch, T. Bein, H. J. Snaith, R. H. Friend, *Nat. Nanotechnol.* **2014**, *9*, 687; b) Y. Hassan, J. H. Park, M. L. Crawford, A. Sadhanala, J. Lee, J. C. Sadighian, E. Mosconi, R. Shivanna, E. Radicchi, M. Jeong, C. Yang, H. Choi, S. H. Park, M. H. Song, F. De Angelis, C. Y. Wong, R. H. Friend, B. R. Lee, H. J. Snaith, *Nature* **2021**, *591*, 72-77; c) T. Chiba, Y. Hayashi, H. Ebe, K. Hoshi, J. Sato, S. Sato, Y.-J. Pu, S. Ohisa, J. Kido, *Nat. Photonics* **2018**, *12*, 681-687; d) Y.-H. Kim, S. Kim, A. Kakekhani, J. Park, J. Park, Y.-H. Lee, H. Xu, S. Nagane, R. B. Wexler, D.-H. Kim, S. H. Jo, L. Martínez-Sarti, P. Tan, A. Sadhanala, G.-S. Park, Y.-W. Kim, B. Hu, H. J. Bolink, S. Yoo, R. H. Friend, A. M. Rappe, T.-W. Lee, *Nat. Photonics* **2021**, *15*, 148-155; e) Z. Xiao, R. A. Kerner, L. Zhao, N. L. Tran, K. M. Lee, T.-W. Koh, G. D. Scholes, B. P. Rand, *Nat. Photonics* **2017**, *11*, 108.

[2] a) D. Ma, K. Lin, Y. Dong, H. Choubisa, A. H. Proppe, D. Wu, Y.-K. Wang, B. Chen, P. Li, J. Z. Fan, F. Yuan, A. Johnston, Y. Liu, Y. Kang, Z.-H. Lu, Z. Wei, E. H. Sargent, *Nature* **2021**, *599*, 594-598; b) K. Lin, J. Xing, L. N. Quan, F. P. G. de Arquer, X. Gong, J. Lu, L. Xie, W. Zhao, D. Zhang, C. Yan, W. Li, X. Liu, Y. Lu, J. Kirman, E. H. Sargent, Q. Xiong, Z. Wei, *Nature* **2018**, *562*, 245-248; c) J. Jiang, Z. Chu, Z. Yin, J. Li, Y. Yang, J. Chen, J. Wu, J. You, X. Zhang, *Adv. Mater.* **2022**, *34*, e2204460; d) Y. Cao, N. Wang, H. Tian, J. Guo, Y. Wei, H. Chen, Y. Miao, W. Zou, K. Pan, Y. He, H. Cao, Y. Ke, M. Xu, Y. Wang, M. Yang, K. Du, Z. Fu, D. Kong, D. Dai, Y. Jin, G. Li, H. Li, Q. Peng, J. Wang, W. Huang, *Nature* **2018**, *562*, 249-253; e) B. Zhao, S. Bai, V. Kim, R. Lamboll, R. Shivanna, F. Auras, J. M. Richter, L. Yang, L. Dai, M. Alsari, X.-J. She, L. Liang, J. Zhang, S. Lilliu, P. Gao, H. J. Snaith, J. Wang, N. C. Greenham, R. H. Friend, D. Di, *Nat. Photonics* **2018**, *12*, 783-789; f) W. Xu, Q. Hu, S. Bai, C. Bao, Y. Miao, Z. Yuan, T. Borzda, A. J. Barker, E. Tyukalova, Z. Hu, M. Kawecki, H. Wang, Z. Yan, X. Liu, X. Shi, K. Uvdal, M. Fahlman, W. Zhang, M. Duchamp, J.-M. Liu, A. Petrozza, J. Wang, L.-M. Liu, W. Huang, F. Gao, *Nat. Photonics* **2019**, *13*, 418-424.

[3] a) Y. Liu, J. Cui, K. Du, H. Tian, Z. He, Q. Zhou, Z. Yang, Y. Deng, D. Chen, X. Zuo, Y. Ren, L. Wang, H. Zhu, B. Zhao, D. Di, J. Wang, R. H. Friend, Y. Jin, *Nat. Photonics* **2019**, *13*, 760-764; b) Y. Dong, Y.-K. Wang, F. Yuan, A. Johnston, Y. Liu, D. Ma, M.-J. Choi, B. Chen, M. Chekini, S.-W. Baek, L. K. Sagar, J. Fan, Y. Hou, M. Wu, S. Lee, B. Sun, S. Hoogland, R. Quintero-Bermudez, H. Ebe, P. Todorovic, F. Dinic, P. Li, H. T. Kung, M. I. Saidaminov, E. Kumacheva, E. Spiecker, L.-S. Liao, O. Voznyy, Z.-H. Lu, E. H. Sargent, *Nat. Nanotechnol.* **2020**, *15*, 668-674.

[4] a) C. Qin, T. Matsushima, W. J. Potscavage, A. S. D. Sandanayaka, M. R. Leyden, F. Bencheikh, K. Goushi, F. Mathevet, B. Heinrich, G. Yumoto, Y. Kanemitsu, C. Adachi, *Nat. Photonics* **2019**, *14*, 70-75; b) N. Wang, L. Cheng, R. Ge, S. Zhang, Y. Miao, W. Zou, C. Yi, Y. Sun, Y. Cao, R. Yang, Y. Wei, Q. Guo, Y. Ke, M. Yu, Y. Jin, Y. Liu, Q. Ding, D. Di, L. Yang, G. Xing, H. Tian, C. Jin, F. Gao, R. H. Friend, J. Wang, W. Huang, *Nat. Photonics* **2016**, *10*, 699; c) M. Yuan, L. N. Quan, R. Comin, G. Walters, R. Sabatini, O. Voznyy, S. Hoogland, Y. Zhao, E. M.

Beauregard, P. Kanjanaboos, Z. Lu, D. H. Kim, E. H. Sargent, *Nat. Nanotechnol.* **2016**, *11*, 872; d) J. Xing, Y. Zhao, M. Askerka, L. N. Quan, X. Gong, W. Zhao, J. Zhao, H. Tan, G. Long, L. Gao, Z. Yang, O. Voznyy, J. Tang, Z.-H. Lu, Q. Xiong, E. H. Sargent, *Nat. Commun.* **2018**, *9*, 3541; e) Y.-K. Wang, D. Ma, F. Yuan, K. Singh, J. M. Pina, A. Johnston, Y. Dong, C. Zhou, B. Chen, B. Sun, H. Ebe, J. Fan, M.-J. Sun, Y. Gao, Z.-H. Lu, O. Voznyy, L.-S. Liao, E. H. Sargent, *Nat.* Commun. **2020**, *11*, 3674; f) Q. Wang, X. Wang, Z. Yang, N. Zhou, Y. Deng, J. Zhao, X. Xiao, P. Rudd, A. Moran, Y. Yan, J. Huang, *Nat. Commun.* **2019**, *10*, 5633.

[5] a) P. Pang, G. Jin, C. Liang, B. Wang, W. Xiang, D. Zhang, J. Xu, W. Hong, Z. Xiao, L. Wang, G. Xing, J. Chen, D. Ma, *ACS Nano* **2020**, *14*, 11420-11430; b) Z. Li, Z. Chen, Y. Yang, Q. Xue, H.-L. Yip, Y. Cao, *Nat. Commun.* **2019**, *10*, 1027; c) Z. Chu, Y. Zhao, F. Ma, C.-X. Zhang, H. Deng, F. Gao, Q. Ye, J. Meng, Z. Yin, X. Zhang, J. You, *Nat. Commun.* **2020**, *11*, 4165.

[6] C. Wang, D. Han, J. Wang, Y. Yang, X. Liu, S. Huang, X. Zhang, S. Chang, K. Wu, H. Zhong, *Nat. Commun.* **2020**, *11*, 6428.

[7] a) N. E. Wright, X. Qin, J. Xu, L. L. Kelly, S. P. Harvey, M. F. Toney, V. Blum, A. D. Stiff-Roberts, *Chem. Mater.* **2022**, *34*, 3109-3122; b) A. J. Knight, L. M. Herz, *Energy Environ. Sci.* **2020**, *13*, 2024-2046.

[8] C. Sun, Y. Jiang, M. Cui, L. Qiao, J. Wei, Y. Huang, L. Zhang, T. He, S. Li, H. Y. Hsu, C. Qin, R. Long, M. Yuan, *Nat. Commun.* **2021**, *12*.

[9] R. Quintero-Bermudez, A. Gold-Parker, A. H. Proppe, R. Munir, Z. Yang, S. O. Kelley, A. Amassian, M. F. Toney, E. H. Sargent, *Nat. Mater.* **2018**, *17*, 900-907.

[10] a) Y. Liu, L. K. Ono, G. Tong, H. Zhang, Y. Qi, *ACS Energy Lett.* **2021**, *6*, 908-914; b) Y. Shang, Y. Liao, Q. Wei, Z. Wang, B. Xiang, Y. Ke, W. Liu, Z. Ning, *Sci. Adv.* **2019**, *5*, eaaw8072.

[11] a) M. Yang, T. Tian, W. Feng, L. Wang, W.-Q. Wu, *Acc. Mater. Res.* **2021**, *2*, 1141-1155; b) M. Kazes, T. Udayabhaskararao, S. Dey, D. Oron, *Acc. Chem. Res.* **2021**, *54*, 1409-1418; c) Y. Xu, W. Xu, Z. Hu, J. A. Steele, Y. Wang, R. Zhang, G. Zheng, X. Li, H. Wang, X. Zhang, E. Solano, M. B. J. Roeffaers, K. Uvdal, J. Qing, W. Zhang, F. Gao, *J. Phys. Chem. Lett.* **2021**, *12*, 5836-5843; d) J. Hu, R. A. Kerner, I. Pelczer, B. P. Rand, J. Schwartz, *ACS Energy Lett.* **2021**, *6*, 2262-2267.

[12] a) S. Ahmad, P. Fu, S. Yu, Q. Yang, X. Liu, X. Wang, X. Wang, X. Guo, C. Li, *Joule* **2019**, *3*, 794-806; b) L. Mao, W. Ke, L. Pedesseau, Y. Wu, C. Katan, J. Even, M. R. Wasielewski, C. C. Stoumpos, M. G. Kanatzidis, *J. Am. Chem. Soc.* **2018**, *140*, 3775-3783; c) T. Steiner, *Angew. Chem. Int. Ed.* **2002**, *41*, 48-76.

[13] a) Y. Liu, L. K. Ono, G. Tong, T. Bu, H. Zhang, C. Ding, W. Zhang, Y. Qi, *J. Am. Chem. Soc.* **2021**, *143*, 19711-19718; b) S. Yuan, Z.-K. Wang, L.-X. Xiao, C.-F. Zhang, S.-Y. Yang, B.-B. Chen, H.-T. Ge, Q.-S. Tian, Y. Jin, L.-S. Liao, *Adv. Mater.* **2019**, *31*, 1904319; c) M. Worku, Q. He, L.-j. Xu, J. Hong, R. X. Yang, L. Z. Tan, B. Ma, *ACS Appl. Mater. Interfaces* **2020**, *12*, 45056-45063; d) X. Peng, B. He, H. Zheng, Z. Su, X. Li, L. Ji, T. Zhang, L. Chen, C. Qin, X. Gao, S. Li, X. Yang, *ACS Energy Lett.* **2023**, *8*, 339-346. *Note, the ref. 13d reported a mixed RP and DJ phase based blue PeLEDs.

[14] R. Zhao, R. P. Sabatini, T. Zhu, S. Wang, A. Morteza Najjarian, A. Johnston, A. J. Lough, S. Hoogland, E. H. Sargent, D. S. Seferos, *J. Am. Chem. Soc.* **2021**, *143*, 19901-19908.

[15] a) E. Shi, B. Yuan, S. B. Shiring, Y. Gao, Akriti, Y. Guo, C. Su, M. Lai, P. Yang, J. Kong, B. M. Savoie, Y. Yu, L. Dou, *Nature* **2020**, *580*, 614-620; b) Akriti, E. Shi, S. B. Shiring, J. Yang, C. L. Atencio-Martinez, B. Yuan, X. Hu, Y. Gao, B. P. Finkenauer, A. J. Pistone, Y. Yu, P. Liao, B. M. Savoie, L. Dou, *Nat. Nanotechnol.* **2021**, *16*, 584-591; c) K. Wang, L. Jin, Y. Gao, A. Liang, B. P. Finkenauer, W. Zhao, Z. Wei, C. Zhu, T.-F. Guo, L. Huang, L. Dou, *ACS Nano* **2021**, *15*, 6316-6325.

[16] K. Wang, Z.-Y. Lin, Z. Zhang, L. Jin, K. Ma, A. H. Coffey, H. R. Atapattu, Y. Gao, J. Y. Park, Z. Wei, B. P. Finkenauer, C. Zhu, X. Meng, S. N. Chowdhury, Z. Chen, T. Terlier, T.-H. Do, Y. Yao, K. R. Graham, A. Boltasseva, T.-F. Guo, L. Huang, H. Gao, B. M. Savoie, L. Dou, *Nat. Commun.* **2023**, *14*, 397.

[17] a) F. Wang, X. Li, H. Duan, H. Wang, L. Fan, Y. Sun, Y. Sui, J. Yang, L. Yang, *Chem. Eng. J.* **2022**, *428*, 132528; b) L. Zhu, H. Cao, C. Xue, H. Zhang, M. Qin, J. Wang, K. Wen, Z. Fu, T. Jiang, L. Xu, Y. Zhang, Y. Cao, C. Tu, J. Zhang, D. Liu, G. Zhang, D.

Kong, N. Fan, G. Li, C. Yi, Q. Peng, J. Chang, X. Lu, N. Wang, W. Huang, J. Wang, *Nat. Commun.* **2021**, *12*, 5081.

[18] a) X. Yang, X. Zhang, J. Deng, Z. Chu, Q. Jiang, J. Meng, P. Wang, L. Zhang, Z. Yin, J. You, *Nat. Commun.* **2018**, *9*, 570; b) J. Ma, L. Yang, Y. Zhang, Y. Kuang, M. Shao, *J. Phys. Chem. Lett.* **2022**, *13*, 4739-4746.

[19] S. J. Hall, P. J. Budden, A. Zats, M. Y. Sfeir, *Rev. Sci. Instrum.* **2023**, *94*, 043005.

[20] A. Liang, K. Wang, Y. Gao, B. P. Finkenauer, C. Zhu, L. Jin, L. Huang, L. Dou, *Angew. Chem. Int. Ed.* **2021**, *60*, 8337-8343.

[21] J. Cho, P. V. Kamat, Adv. *Opt. Mater.* **2021**, *9*, 2001440.

[22] B. Wang, Y.-H. Zhou, S. Yuan, Y.-H. Lou, K.-L. Wang, Y. Xia, C.-H. Chen, J. Chen, Y.-R. Shi, Z.-K. Wang, L.-S. Liao, *Angew. Chem. Int. Ed.* **2023**, *62*, e202219255.

[23] W. Zhou, Y. Shen, L.-X. Cao, Y. Lu, Y.-Y. Tang, K. Zhang, H. Ren, F.-M. Xie, Y.-Q. Li, J.-X. Tang, *Adv. Funct. Mater.* **2023**, 2301425.

COMMUNICATION

WILEY-VCH

Entry for the Table of Contents
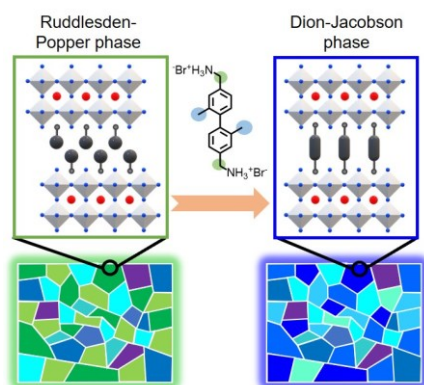
New di-ammonium ligands with rigid π-conjugated rings and additional methyl groups were designed and synthesized to construct DJ perovskite structures. This leads to reduced energetic disorders in blue emissive films with improved optoelectronic properties. On this basis, we can demonstrate DJ PeLEDs with a peak EQE of ~4% at 484 nm and ~11% at 494 nm, which are among the top reported for pure DJ phase based PeLEDs in the corresponding wavelength regions.